

Biomechanical evaluation of a novel glenoid design in total shoulder arthroplasty

Vincent M. Wang, PhD,^a Ramaswamy Krishnan, MS,^b Obinwanne F. C. Ugwonalu, MD,^c Evan L. Flatow, MD,^a Louis U. Bigliani, MD,^c and Gerard A. Ateshian, PhD,^b New York, NY

The amount of articular curvature mismatch providing optimal performance in total shoulder arthroplasty (TSA) is unknown. The objectives of this study were to quantify glenohumeral joint mechanics before and after TSA and to compare the performance of 3 glenoid components: (1) nonconforming, (2) conforming, and (3) a novel design featuring a conforming center extending into a nonconforming periphery. Six fresh-frozen cadaveric shoulders (mean age, 43 years) were mechanically tested on a custom apparatus by use of simulated muscle forces and a coordinate-measuring machine to determine joint kinematics. B-spline models of the natural and prosthetic articular surfaces were generated, and joint contact was computed by use of a proximity criterion. During both centered ($P = .02$) and eccentric ($P = .05$) loading protocols, glenoid contact migrated posteriorly in conforming implants. No statistical differences in kinematics and contact were found among the nonconforming design, the new design, and the natural joint. Therefore, adding a central region of conformity does not compromise the ability of nonconforming TSA components to reduce rim loading. (J Shoulder Elbow Surg 2005;14:129S-140S.)

Prosthesis replacement of the glenohumeral joint (GHJ) articular surfaces is a highly successful surgical technique performed for pain relief and restoration of normal joint function, with greater than 90% of total

From the Leni and Peter W. May Department of Orthopaedics, Mount Sinai School of Medicine, Department of Mechanical Engineering, Columbia University, and Department of Orthopaedic Surgery and the Shoulder Service, Columbia-Presbyterian Medical Center.

This study was supported by a research grant from Zimmer, Inc (G.A.A.).

Reprint requests: Gerard A. Ateshian, PhD, Professor of Mechanical Engineering and Biomedical Engineering, Columbia University, Department of Mechanical Engineering, 500 West 120th St, 220 SW Mudd, MC 4703, New York, NY 10027-6699 (E-mail: ateshian@columbia.edu).

Copyright © 2005 by Journal of Shoulder and Elbow Surgery Board of Trustees.

1058-2746/2005/\$30.00

doi:10.1016/j.jse.2004.09.029

shoulder arthroplasty (TSA) procedures providing satisfactory results with a relatively low revision rate.^{5,6,11,14,25,26,30,38,42} Common indications for arthroplasty include osteoarthritis (primary or secondary), rheumatoid arthritis, trauma, avascular necrosis, and cuff tear arthropathy.³⁹ Neer's conforming prosthesis enjoyed widespread popularity and success upon its introduction in the mid 1970s and featured a humeral head and glenoid component with equal radii of curvature.³⁹ In retrospective studies of patients fitted with conforming implants, loosening of the glenoid component, though rare, is the most common complication of TSA, with studies suggesting a mean incidence of 5% for a mean follow-up time of 3 to 5 years.^{12,40,53}

The prevalence of nonconforming GHJ implants has risen dramatically as surgeons seek to reduce the incidence of glenoid loosening and joint instability; indeed, fully nonconforming glenohumeral prosthetic components (in which the radius of curvature of the humeral head is smaller than that of the glenoid)^{9,10} have become the preferred choice among many orthopaedic surgeons today. Still, major controversy exists with regard to selection of the optimal degree of glenohumeral mismatch in TSA. A conforming design ideally minimizes humeral head translations and provides maximal contact area with the glenoid. However, in extreme arm positions, such as hyperextension or flexion or with pathologic conditions such as rotator cuff tears,^{15,19,43} subluxation of the humeral head may lead to rim loading of the glenoid and produce an undesired mechanical moment—the so-called rocking-horse effect.^{5,20,32,34,44} In contrast, a nonconforming joint theoretically allows for some humeral head subluxation without rim loading; however, the relative contact area is decreased, and consequently, a higher contact stress is transmitted to the glenoid component. This increase in stress can lead to greater polyethylene deformation and wear or even catastrophic failure of the component.¹⁸ To integrate the perceived advantages of both the conforming and nonconforming designs, 2 of us (L.U.B. and E.L.F.) recently developed a novel glenoid, the Bigliani-Flatow (BF) design,⁵⁴ a hybrid design featuring an articular surface with 2 distinct radii of curvature: an inner, perfectly congruent region extending

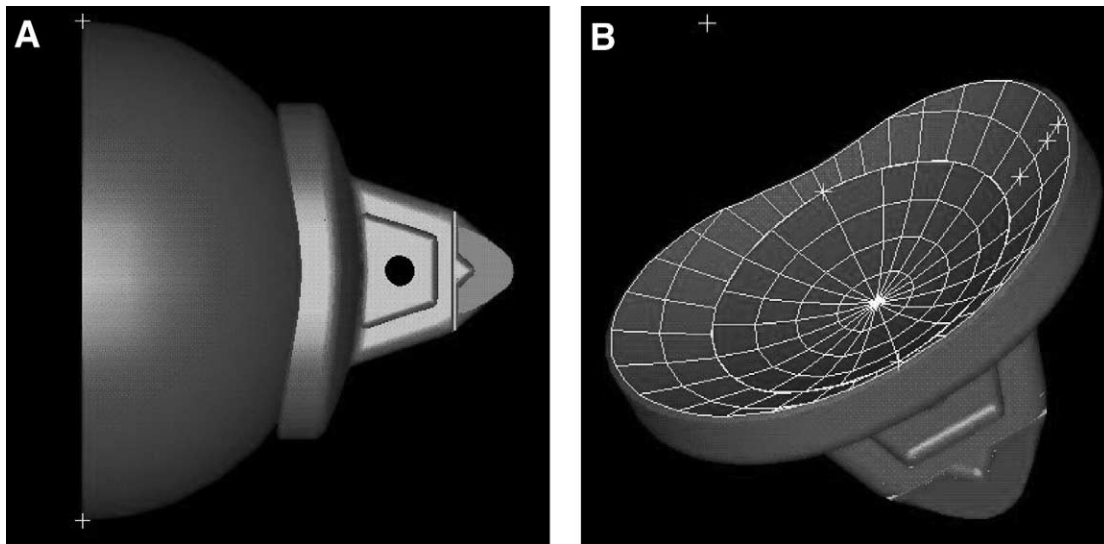


Figure 1 Computer representations of BF glenoid. Note the glenoid's central region of conformity and peripheral region of nonconformity in both the side (A) and articular (B) views.

into an outer, incongruent region or "translation zone" (Figure 1).

Previous experimental investigations of shoulder arthroplasty biomechanics have studied the role of component conformity on joint stability. Friedman²² observed posterior humeral migration during flexion-extension movements in patients with conforming glenohumeral prostheses. Karduna et al³³ reported that dislocation forces were significantly affected by component conformity, although the differences were small (3%). This study implied that the wall length was the most important factor in determining joint stability. The same authors found that, on average, prosthetic components of less conformity tended to better replicate the kinematic patterns of the natural joint.³² Karduna et al³⁴ and Anglin et al¹ conducted analyses on the load-deformation response of GHJ implants of varying conformity and showed favorable agreement between their experimental results and theoretic predictions from rigid-body mechanics. Whereas the effects of component size, conformity, and constraint on glenohumeral stability have been separately studied in numerous cadaveric models,^{1,8,27,32-34,45,49} few, if any, experimental studies have examined changes in prosthetic articular contact patterns associated with varying component conformity. As small humeral head translations can dramatically affect the location and size of the corresponding glenoid contact area,¹⁷ studying contact patterns after TSA may facilitate the localization of glenoid edge loading. Moreover, by simultaneously studying the kinematics, glenoid contact areas, and resultant GHJ forces after TSA, the consequences of altering component conformity may be more fully understood.

In previous unpublished finite-element studies, we examined the peak von Mises stresses for conforming and nonconforming glenohumeral components, as well as for the new BF design, under conditions of both centered loading (750 N) and prescribed posterior humeral head subluxation. When the head was centered in the glenoid, the nonconforming components (ie, 3-mm radius of curvature mismatch) experienced elevated peak stresses (10 MPa) compared with the conforming (approximately 1 MPa) and BF (1.3 MPa) designs. After an imposed humeral posterior subluxation of 1.0 mm, the peak von Mises stresses for the BF design (30.8 MPa) were found to be intermediate to those of the nonconforming (11.5 MPa) and conforming (43.2 MPa) designs. These finite-element analyses assumed a linear stress-strain response for ultrahigh-molecular weight polyethylene (Young's modulus, $E_Y = 930$ MPa; Poisson's ratio, $\nu = 0.46$) and did not account for stress yielding or creep. To supplement these data in a more clinically relevant fashion, we expanded our studies to a cadaveric shoulder model using muscle forces to position the humeral head on the glenoid so that the resulting kinematics and contact patterns could be determined experimentally.

The objective of the present study is to quantify and compare normal GHJ mechanics with that after TSA with 3 separate glenoid components: a perfectly conforming glenoid, a nonconforming glenoid, and the BF design. The specific aims of this investigation are to quantify the kinematics of the humeral head, the articular contact of the humeral head on the glenoid, and the resultant joint forces associated with both natural and prosthetic joints and to evaluate the effect

of articular-surface conformity on joint stability under conditions of both centered and eccentric joint loading. We hypothesized that elevation in the scapular plane, representing a mode of centered joint loading, would produce minimal translations of the humeral head and centered contact on the glenoid. For eccentric positions outside of the scapular plane, we hypothesized that contact would occur closer to the glenoid rim in conforming joints in comparison to nonconforming joints, with the BF design exhibiting an intermediate response.

MATERIALS AND METHODS

The experimental model used in this study is based on that developed by Soslowky et al⁴⁷ for glenohumeral contact studies and adapted by Kelkar et al³⁶ for kinematic studies.

Specimen preparation

Six fresh-frozen cadaveric shoulders (mean age, 43 ± 12 years; range, 22-54 years) were tested in this study. All shoulders underwent radiography and were examined for evidence of fractures, osteoarthritis, or bony abnormalities, which would otherwise render them inadequate for inclusion in the study. Furthermore, any specimen found to have soft-tissue pathology (ie, rotator cuff tear or evidence of prior surgery) or that demonstrated an abnormal limited range of motion at the time of dissection was also excluded.

After a 12-hour thawing process, each shoulder was dissected down to the GHJ, removing all soft tissue except for the subacromial bursa, coracohumeral and coracoacromial ligaments, and deltoid and rotator cuff muscles. During dissection, preparation, and testing, the joint was regularly moistened with a physiologic saline solution to retard specimen degradation. The muscle bellies of the supraspinatus, infraspinatus, teres minor, and subscapularis were dissected off the scapula and upon careful inspection of their muscle fiber directions, an eye screw was placed at the approximate centroid of each muscle origin near the medial border of the scapula. Dissection of rotator cuffs proceeded laterally, and their tendons were carefully separated from the underlying and confluent joint capsule by use of sharp dissection, with care taken to preserve their insertions on the proximal humeral tuberosities. Each rotator cuff muscle was then transected 3 to 4 mm medial to its musculotendinous junction, and a woven Dacron strip was sutured to the medial tendon edge. Because of their similar lines of action and adjacent insertion sites, the infraspinatus and teres minor were modeled as a single, summed musculotendinous unit. To simulate the rotator cuff lines of action, small triangular clamps were first looped through the Dacron strips to provide uniform loading across the tendon width. Flexible cables were then secured to each clamp, threaded through the eye screws on the scapula, and redirected over pulleys to worm gear mechanisms in series with calibrated spring scales. The precise tensile force applied to each tendon in all testing positions was recorded from the spring scales (resolution, 0.6 N) for subsequent calculation of resultant joint forces.

The 3 muscle bellies of the deltoid (anterior, middle, and

posterior) were identified and traced to their origins along the distal clavicle, acromion, and scapular spine. The centroid of each of the 3 origins was marked on the bone and the origin of the entire deltoid resected. Each third of the deltoid was sharply dissected off its insertion on the distal humerus while the distally extending footprint of the insertion was marked with India ink as it was resected. Then a cortical bone screw was drilled through the humerus at the centroid of the 3 distal-most tendon insertions. To simulate the anatomic lines of action of the deltoid, flexible cables affixed to the cortical screws at the deltoid insertions were routed through eyebolts positioned at the approximate anatomic origin of each head of the deltoid and redirected over pulleys to worm gear mechanisms in series with calibrated spring scales.

A lightweight alignment plate was attached to the distal humerus to facilitate measurement of the angle of humeral rotation. The glenohumeral abduction angle was measured during experimentation with a goniometer centered behind the humeral head. The lower third of the scapula was potted in polymethyl methacrylate (PMMA) cement with the plane of the scapula tilted anteriorly by 20° and its medial border vertical, to simulate its *in vivo* orientation with the arm at the side.^{36,47} The joint was then mounted onto a custom joint-testing rig²⁴ that facilitated the experimental modeling and measurement of GHJ motion.³⁵

Both the scapula and humerus were instrumented with 2 rigid triads for geometric and kinematic analyses.^{35,51} On the scapula, triads were placed in the scapular spine near the acromion as well as in the anterior coracoid; to accommodate the length of the stem used for the humeral prosthesis, the more proximal of the 2 humeral triads was typically inserted 140 mm from the articular margin of the humeral head. Each triad consisted of three 6.35-mm-diameter precision metallic spheres (Industrial Tectonics, Inc, Dexter, MI).

On the basis of anthropometric data for a 68.2-kg human being (representing a mean weight of male and female subjects), a 3.1-kg mass simulating the weight of the entire arm was attached at its center of gravity, 25.7 cm from the proximal end of the humerus.⁵² As the scapula remained stationary during testing, scapulothoracic motion was simulated by adjusting the line of action of the arm weight vector originating from the distal humerus at each position of elevation.^{36,47} Glenohumeral abduction angles were converted to total arm elevations in accordance with previous reports.^{16,21,43}

Muscle loading

For each shoulder, the natural joint was actively positioned in each of 7 orientations (described below) by use of coordinated muscle force application. The patterns of muscle loading incorporated during testing were based on reported electromyographic data and muscle lever arms.^{37,41} The joint capsule was vented in each shoulder to eliminate the effect of loss of intraarticular pressure that occurs at higher elevations.

As the principal objective of this investigation was to quantify the differences in GHJ mechanics associated solely with changes in articular geometry, the applied muscle loads used for the natural joint configuration were consistently maintained across all testing configurations in a

Table I Mean applied muscle forces at each test position (n = 6 specimens)

Test position	Subscapularis (N)	Supraspinatus (N)	Infraspinatus (N)	Anterior deltoid (N)	Middle deltoid (N)	Posterior deltoid (N)
SSR at 30°	15.8 ± 2.3	32.6 ± 5.6	14.7 ± 3.8	28.5 ± 6.4	30.7 ± 6.1	22.8 ± 6.5
SSR at 90°	13.7 ± 2.6	61.2 ± 11.5	18.2 ± 3.5	54.9 ± 16.4	54.4 ± 7.4	22.1 ± 11.9
SSR at 120°	14.2 ± 5.3	48.1 ± 10.5	19.3 ± 3.1	54.0 ± 19.1	48.5 ± 5.3	20.8 ± 10.9
SSR at 150°	13.6 ± 4.0	45.3 ± 19.6	22.7 ± 8.8	59.5 ± 19.5	46.2 ± 12.7	17.0 ± 6.7
ESR at 90°	17.9 ± 6.5	58.3 ± 14.1	27.5 ± 6.8	29.9 ± 10.0	58.1 ± 7.0	46.4 ± 8.3
SIR at 90°	42.8 ± 5.3	56.4 ± 14.6	16.8 ± 4.8	34.3 ± 12.0	59.7 ± 9.2	34.9 ± 3.3
FIR at 90°	45.3 ± 8.6	52.7 ± 13.9	17.2 ± 6.1	62.6 ± 13.5	48.5 ± 11.8	22.3 ± 9.6

Labels for test positions indicate humeral orientation and arm elevation angle.

particular specimen. The mean muscle forces for each test position are listed in Table I. After testing of the natural joint, a passive-assisted active loading protocol was implemented, whereby the shoulder was manually (ie, passively) positioned while muscle forces were adjusted toward their targeted values. For a given test position, adjustments to within 10% of the standard force for a particular tendon were permitted to maintain the desired elevation and rotation. With the exception of 1 test position for the conforming prosthesis of specimen 1, the standard load criterion was uniformly satisfied.

Joint loading and kinematic measurement

A coordinate-measuring machine (CMM) (No. CX-652-D2; Mitutoyo, Paramus, NJ) with a rated accuracy of 50 μ m per axis was used to identify the precise location and orientation of both the humerus and the scapula throughout testing.^{35,51} The CMM axes were visually aligned with the anatomic axes of the scapula before testing. At each test position, the 3 spheres on each humeral and scapular triad were digitized for post-experimental kinematic and joint contact analyses. During digitization, the coordinates of the sphere centers were automatically computed and written to a data file on a personal computer interfaced with the CMM.

A 6-degree-of-freedom load transducer (JR3, Inc, Woodland, CA) with repeatability better than 3 N (load) and 20 N-cm (torque) per axis was secured to the specimen-mounting pipe, offset medially from the scapula, to measure the resultant force and moment vector components resulting from external loads applied to the specimen-mounting pipe during testing. Very good agreement was found between the measured and calculated resultant force vector components for each anatomic axis, thus providing confidence in the resultant joint force computations. The equations of the linear regressions relating computed (y) to measured (x) forces were as follows: $y = 0.99x + 6.51$ ($R^2 = 0.98$, $P < .001$) (medial-lateral [M-L]), $y = 0.99x + 3.85$ ($R^2 = 0.93$, $P < .001$) (superior-inferior [S-I]), and $y = 0.96x + 1.69$ ($R^2 = 0.95$, $P < .001$) (anterior-posterior [A-P]). The resultant joint force data reported in this investigation are those after adjustment to measured values in accordance with the regression equations.

Resultant joint force calculation

The GHJ reaction force was calculated for each test position based on a free-body diagram analysis of the

humerus in its experimental configuration. To satisfy static equilibrium (ie, sum of vector forces = 0), the joint reaction force must counteract the resultant force due to (1) the vector sum of the 3 rotator cuff forces, (2) the vector sum of the 3 deltoid forces, and (3) the force resulting from the weight of the arm acting at the distal humerus. Post-experimentally, after joint disarticulation, muscle origins and insertions were digitized together with their associated triads such that the calculated centroids could be transformed to their in situ coordinates. For each test position, force vectors for each individual muscle were computed from the 3-dimensional coordinates of its insertion and origin and by multiplying the unit vector by the magnitude of the applied force. Vectors representing the forces resulting from the weight of the arm were calculated by use of data recorded from digitization of the arm weight cable at each kinematic position during experimentation. Forces due to capsular tension or impingement of the rotator cuff tendons beneath the acromion were neither measured nor modeled. However, on the basis of the above equations demonstrating close agreement between measured and computed joint forces, we believe that the potential contributions of capsular and impingement forces were small.

Test protocol

On the basis of our laboratory and clinical experience, as well as the literature on GHJ kinematics,^{7,28,29,31,36,51} a total of 7 test positions were selected for the experimental protocol. To test our hypotheses for concentric loading, 30°, 90°, 120°, and 150° of scapular-plane arm elevation were chosen on the basis of our previous kinematic studies,^{36,51} which demonstrated minimal translation of the humeral head center of curvature. These arm elevations were performed in starting rotation (SR),^{36,47} which is the amount of external humeral rotation allowing maximal abduction in the scapular plane. An at-risk elevation angle for patients with instability, 90° arm elevation, was selected for the following 3 eccentric loading positions: horizontal extension in starting rotation (ESR), internal rotation in the scapular plane (SIR), and forward flexion with internal rotation (FIR). Flexion and extension were oriented approximately 30° anterior and posterior from the scapular plane, respectively. These 3 test positions were expected to translate the humeral head along the anterior-posterior axis of the joint^{28,29,51} to produce loading near or at the glenoid rim.

To accommodate the study design, which featured biomechanical testing of 3 prosthetic glenoids per specimen, the joint capsule was incised and immediately repaired.

Suture loops were sewn along the incised edges of the capsule and then secured to eye screws inserted in the scapular neck; the length of each loop was adjusted such that the approximate tension of the intact capsule was restored for each test configuration. The extent to which the capsular repair restored the distribution of tension within the capsule was not evaluated quantitatively. Rather, a qualitative comparison was performed to verify that the passive range of rotation and elevation were preserved after capsular release and repair. In all experiments we could not detect an alteration of capsular tension throughout the duration of the entire testing protocol. The capsular repair allowed the replacement of multiple glenoid prostheses and facilitated the restoration of capsular tension for all test positions. After capsular repair, the natural joint was tested first, and the kinematics and force transducer readings were recorded for the 7 test positions described above. Stereophotogrammetry (SPG) was then performed on the glenoid and humeral head cartilage surfaces^{2,46} to quantify their articular-surface topographies for joint contact and kinematic analyses.^{3,36,47} During SPG, the joint remained rigidly mounted to the testing rig to preserve the orientation of the simulated muscle forces.

TSA

After SPG, GHJ replacement was performed by use of standard arthroplasty techniques, as detailed by Zimmer, Inc (Warsaw, IN).⁵⁴ For each specimen, a standard-sized cobalt-chromium-alloy humeral head component of either 18 or 21 mm in thickness with a radius of curvature of 23 or 26 mm was selected. Keeled, ultrahigh-molecular weight polyethylene glenoid components were used, with uniform radii of curvature of 23, 26, or 29 mm (representing conforming and nonconforming articulations with the humeral head components), whereas the available BF glenoids exhibited a central region radius of curvature of 23 or 26 mm. Uniform curvature glenoid components were custom made by Zimmer, Inc and shared the same keel design as the BF. In this study, for a humeral head component with radius of curvature R_H , the corresponding radii of mating conforming and nonconforming glenoids were defined as R_H and $R_H + 3$, respectively. Among the 6 specimens tested, 3 were fitted with humeral components measuring 21 × 46 mm (head height and head diameter, respectively), 2 were 18 × 46 mm, and 1 was 21 × 52 mm.

To prepare the specimens for prosthetic implantation, each GHJ was disarticulated and the incised capsule was reflected laterally and secured with sutures beneath the margins of the humeral articular surface. A custom alignment guide⁵⁴ was inserted onto the humeral reamer to facilitate anatomic resection of the native humeral head at a head-shaft angle of 135° while maintaining 30° of humeral retroversion. Immediately after selection of the prosthetic head, 3 glenoids—conforming, nonconforming, and BF—were randomly assigned the generic labels A, B, and C by a single investigator. A different investigator, blinded to the identities of glenoids A, B, and C, then selected the testing sequence (eg, C-A-B) for these components. After removal of the native glenoid articular cartilage and reaming of the glenoid fossa to a uniform radius of curvature matching that of the back of the glenoid component, the first keeled glenoid was cemented into place. The technique of cement-

ing, removing, and recementing multiple glenoids was refined during our pilot experiments. When the first 2 glenoids were implanted in each specimen, a conservative amount of cement was used for fixation. A 90-minute period was allocated for curing of the bone cement before kinematic testing of each glenoid component. Our PMMA preparation resulted in minimal bone loss, and therefore, subsequent components could be consistently implanted within the bony vault. No visual glenoid loosening was detected during any of the experiments.

Surface registration of implants

After the 7 kinematic positions were tested in the first TSA preparation, the joint capsule was reopened and the humerus reflected superiorly to expose the glenoid surface. The CMM was used to digitize points on the articular and side surfaces of each glenoid component, as well as the coordinates of the spheres fixed to the scapular triads, for subsequent surface registration. After digitizing, the glenoid was removed, and the glenoid vault was prepared for implantation of the second glenoid component, which was tested by use of the identical protocol as the natural joint and first implant; this procedure was again repeated for the final glenoid. At the conclusion of testing, the capsule was fully resected, the joint was disarticulated, and the prosthetic humeral head was digitized along with its reference triads. Typically, prosthetic surface registration required digitizing a minimum of 150 and 80 points on each humeral head and glenoid, respectively.

Calculation of joint kinematics and contact areas

Natural joint surfaces. For the natural joint configuration, the relative positions of the glenoid and humeral head articular surfaces during experimentation were determined by use of the methodology described by Kelkar et al.³⁶ From SPG analysis, 3-dimensional geometric models of the glenoid and humeral head were obtained with their associated humeral and scapular triad coordinates. By use of a least squares optimization procedure, the spatial orientation of both the humeral head and glenoid cartilage surfaces, as well as the coordinates of their centers of curvature, was determined for each respective test position.^{36,47} In situ joint contact areas were calculated by use of the proximity criterion described previously.⁴

Prosthetic components. To conduct kinematic and contact analyses of the implants, accurate geometric models of the GHJ prosthetic components were first created before their use in experiments. After articular curvature measurements were recorded from a CMM with a rated accuracy of 5 μm per axis (MicroVal 343; Brown and Sharpe, North Kingstown, RI), models were constructed by use of I-DEAS Master Series 7.0 solid modeling software (Electronic Data Systems, Plano, TX).

A series of sequential surface alignment procedures was performed to align the glenoid and humeral component surfaces into each of their respective in situ testing positions. In each test configuration, to obtain the orientation (and center of curvature) of the glenoid and humeral head components relative to their scapular and humeral reference triads, respectively, a least squares optimization technique was used to align their corresponding I-DEAS model to the points obtained from direct digitization of these prosthetic

components. To provide a common reference frame for the purpose of reporting results, all prosthetic and natural joint surfaces were aligned to the 90° scapular-plane SR position in the natural joint configuration.

Kinematic reference points. Reference points for kinematic calculations were obtained after alignment of the SPG or I-DEAS model of each glenoid to its experimental in situ position. The anatomic axes for the natural joint configuration were taken to be those of the CMM, as it was not possible to select a nonarbitrary set of coordinate axes for the SPG surfaces (which are portions of spheres). In contrast, anatomic axes were easily assigned to the computer models of the prosthetic glenoid components because of the geometry of these designs (ie, lengths > widths).

In the natural joint, the reference point for reporting translations of the humeral head on a stationary glenoid was computed from the following formulas (valid for left shoulders):

$$c_{ML} = a_{ML} + (R_G - R_H)\cos\alpha$$

$$c_{SI} = a_{SI}$$

$$c_{AP} = a_{AP} - (R_G - R_H)\sin\alpha$$

in which c_{ML} , c_{SI} , and c_{AP} are the M-L, S-I, and A-P coordinates of the reference point, respectively, and a_{ML} , a_{SI} , and a_{AP} are the coordinates of the glenoid center of curvature. R_G and R_H are the radii of curvature of the glenoid and humeral head articular surfaces, respectively, and α is the glenoid retroversion.

The reference point for the conforming prosthetic glenoid and the BF (whose central region is congruent with the humeral head) was the center of curvature of the glenoid component. For nonconforming implants, the reference point c_{gi} was adjusted by an amount proportional to the radial mismatch by use of the following formula (valid for left shoulders):

$$(c_{gi})_m = (c_{gc})_m + (R_G - R_H)n_m$$

in which c_{gc} is the center of curvature of a congruent glenoid, and n is the unit normal of the (nonconforming) glenoid surface. The subscript m denotes the anatomic directions (M-L, S-I, and A-P) for each implanted glenoid. The results from right shoulders were converted to left-shoulder equivalents for comparison purposes.

Statistical analysis

A generalized linear model analysis of variance with repeated measures was performed by use of SAS for Windows (version 8.0; SAS Institute, Cary, NC). The statistical factors were test configuration (natural joint and 3 glenoid types) and arm position (30°, 90°, 120°, and 150° for centered loading and ESR, SIR, and FIR for eccentric loading), whereas the dependent variables included the component resultant joint forces, humeral head translations, and glenoid contact area centroids. When significant differences were detected by use of the generalized linear

model, a Student-Newman-Keuls multiple-range comparison was used to detect differences among levels of a factor. Group means for the 3 implant configurations were computed for statistical comparisons (ie, paired t tests) between natural and prosthetic joints. Statistical significance was assumed for $P < .05$.

RESULTS

Resultant joint forces

For the concentric loading positions, no significant differences ($P > .4$) were found among test configurations for the total resultant force magnitude or for the M-L, S-I, or A-P resultant force components. Similarly, no significant differences could be detected among total resultant forces ($P = .35$) or the M-L ($P = .45$) and S-I ($P = .28$) force components when eccentric loading positions were analyzed. However, A-P forces demonstrated significant differences in the FIR position, as nonconforming implants experienced more posteriorly directed forces (52 ± 23 N) when compared with the natural joints (35 ± 18 N) ($P = .037$). Across all test configurations, the mean total resultant force magnitude ranged from a minimum value of 81 ± 12 N (30°, nonconforming implant) to a maximum value of 194 ± 16 N (flexion with internal rotation, conforming implant).

Humeral head translation

During centered loading, the kinematics of the center of curvature of the humeral head was similar among natural and prosthetic glenoids, with the exception of the conforming prosthesis, which tracked significantly posteriorly ($P = .005$), particularly in the mid-range elevations (Figure 2, A). For all glenoids, the humeral head tended to migrate anteroinferiorly with elevation in the scapular plane (Figure 2). The mean position of the humeral head center was more superior with prosthetic glenoids in comparison to the natural joint (3.7 ± 3.8 mm vs 2.2 ± 2.6 mm, $P = .017$). Though not statistically significant, natural joints tended to track more anteriorly compared with implants (1.5 ± 3.0 mm vs 0.8 ± 2.0 mm, $P = .09$).

During eccentric loading, all 3 glenoid designs promoted similar kinematics to that of the natural joint (Figure 3). For all glenoids, characteristic trends were observed in the A-P direction, with progressive ($P < .02$) posterior translation observed as the humerus was moved from extension into flexion (Figure 3, A). Contrary to our hypothesis, A-P translations for the conforming glenoid were similar to the BF, nonconforming, and natural joint ($P = .27$). Similar to the centered loading mode, implants translated more superiorly than the natural joint (4.1 ± 4.0 mm vs 1.6 ± 2.9 mm, $P = .001$) under conditions of eccentric loading. However, A-P translations were very similar

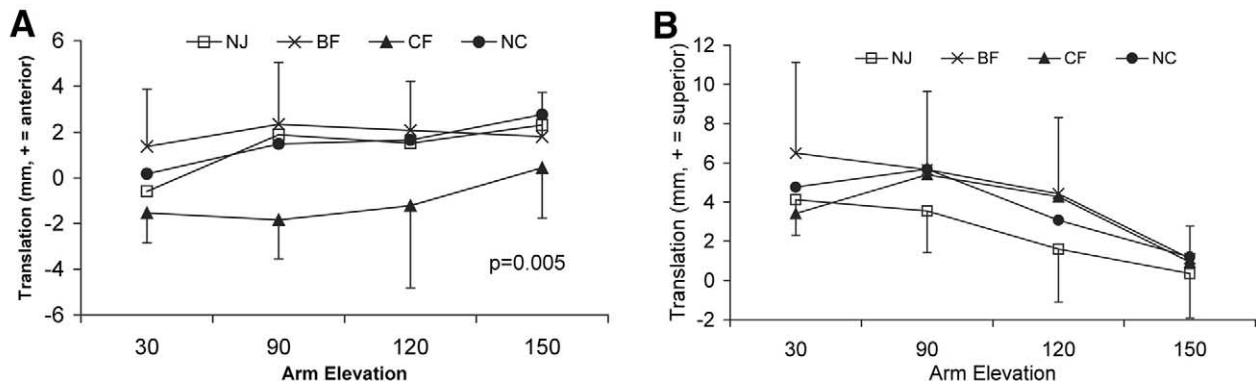


Figure 2 Mean A-P (A) and S-I (B) translation of the center of curvature of the humeral head during concentric loading. Error bars represent SDs. NJ, Natural joint; CF, conforming; NC, nonconforming.

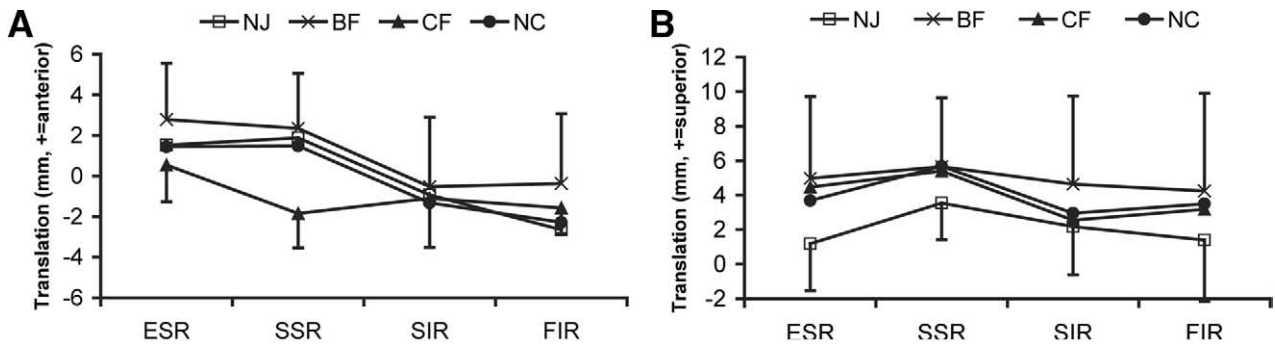


Figure 3 Mean A-P (A) and S-I (B) translation of the center of curvature of the humeral head during eccentric loading. Error bars represent SDs. NJ, Natural joint; CF, conforming; NC, nonconforming.

($P > .9$) between prosthetic and natural joints (mean posterior translation, 0.5 mm).

Glenoid contact centroids

Centroids for the prosthetic glenoid contact areas are presented in the anatomic coordinate system of their I-DEAS models. For consistency, the contact centroids in the natural joint were likewise expressed in this coordinate system. During concentric loading, the contact area centroid behaved similarly to the motion of the center of the humeral head. For the nonconforming, BF, and natural joints, the contact centroid remained centered or slightly anterior as well as superior to the joint center (Figure 4). However, the conforming glenoid demonstrated statistically significant ($P = .02$) posterior contact (Figure 4, A), consistent with the kinematic findings. S-I centroid translations were not influenced by glenoid type ($P > .3$) (Figure 4, B). Glenoid contact in implants was significantly more posterior than in the natural joints (-1.2 ± 4.4 mm vs 1.6 ± 3.8 mm, $P = .001$), whereas S-I centroids were approximately the same ($P > .8$; mean superior location, 8.8 mm).

Movement of the humerus from extension to flexion

caused the centroid to migrate posteriorly ($P = .0006$) and inferiorly ($P = .003$) for all glenoid configurations (Figure 5). The conforming glenoid produced significantly ($P = .05$) more posterior contact than the natural joint, particularly in the position of flexion with internal rotation, where the contact occurred closer to the rim (Figures 5, A and 6). Interestingly, in all cases joint contact was predominantly in the superior region of the glenoid component (Figure 5, B). Prosthetic joint contact centroids were more superior (8.3 ± 5.3 mm vs 4.8 ± 6.2 mm, $P = .069$) and significantly more posterior (-3.2 ± 4.9 mm vs -0.4 ± 5.6 mm, $P = .0038$) than for natural joints.

DISCUSSION

Foremost among the objectives of total shoulder replacement are to restore motion and strength and to eliminate pain. Over the past 3 decades, modern TSA has been highly successful in the treatment of GHJ degeneration. However, there remains considerable controversy in determining the amount of component conformity that optimizes implant performance in

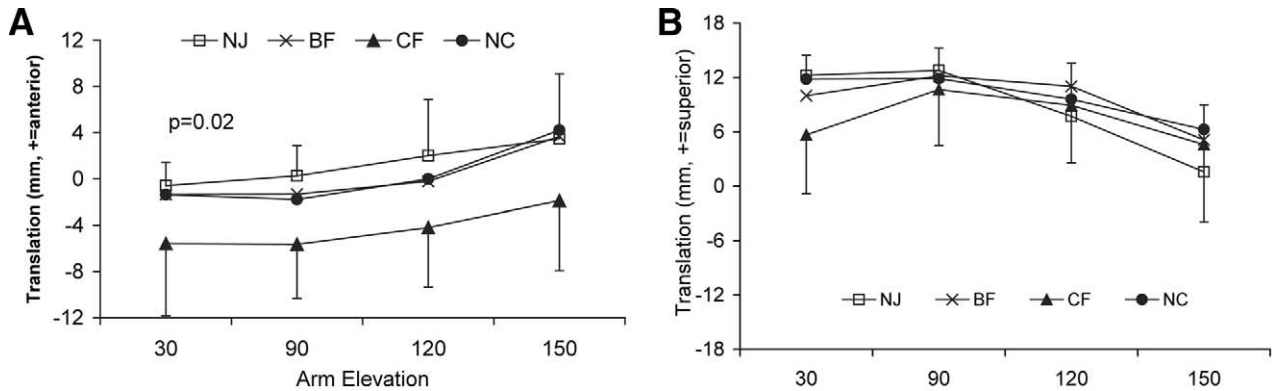


Figure 4 Mean A-P (**A**) and S-I (**B**) translation of glenoid contact centroid during concentric loading. In these line graphs, the y-axes correspond to the typical 24-mm A-P width or 36-mm S-I length of the prosthetic glenoids, with 0 mm of translation indicating the glenoid center for each axis. Error bars represent SDs. NJ, Natural joint; CF, conforming; NC, nonconforming.

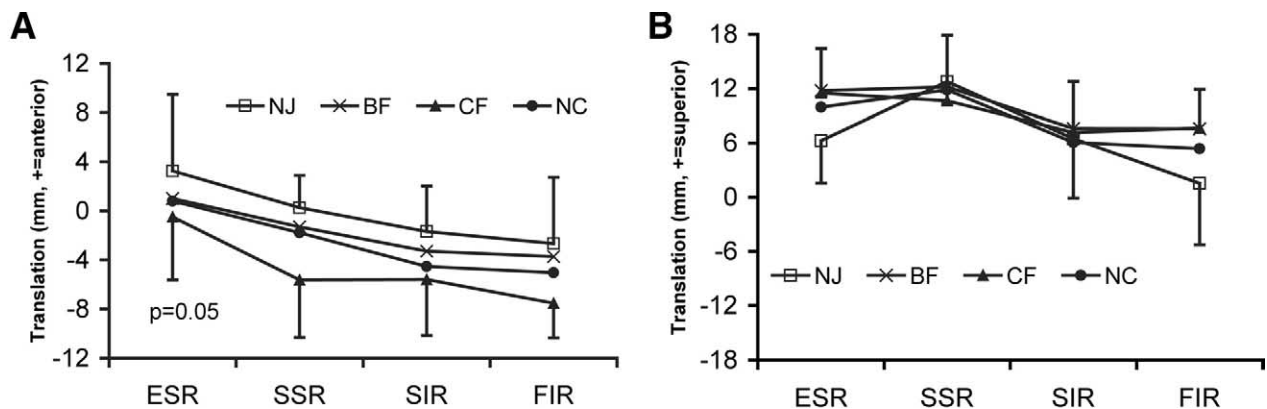


Figure 5 Mean A-P (**A**) and S-I (**B**) translation of glenoid contact centroid during eccentric loading. Error bars represent SDs. NJ, Natural joint; CF, conforming; NC, nonconforming.

vivo. Neer's original unconstrained TSA design featuring conforming glenohumeral components has long been considered the standard for GHJ replacement because of its clinical efficacy and durability.^{11,38,48} Today, long-term follow-up studies continue to cite glenoid component loosening as the most frequent indication for revision surgery.^{13,53} These results may be responsible for shoulder surgeons' increasing preference for nonconforming components (which, by design, are less likely to produce glenoid rim loading) despite the risk of increased contact stresses during centered loading. Recently, the innovative BF glenoid design (Zimmer, Inc) was introduced, featuring a conforming central geometry and nonconforming peripheral region, in contrast to other designs that are either fully conforming or fully nonconforming. The present study is among the first reports assessing ex vivo joint biomechanics after shoulder arthroplasty with the BF system.

The experimental protocol developed for this study

included test positions (30°-150° arm elevation) in the scapular plane that we hypothesized would produce minimal translations and centered joint contact with no significant differences among glenoid implants. Throughout elevation in the scapular plane, the contact centroid for the conforming glenoid was displaced posteriorly ($P = .017$) by 3 mm or more relative to the natural joint, the BF, and the nonconforming glenoids, which demonstrated centered contact over these same elevations (Figure 4, A). An equally surprising finding was that conforming joints exhibited a marked and significant ($P = .005$) (Figure 2, A) posterior translation during concentric loading. S-I translations, meanwhile, demonstrated similar kinematic patterns among the implants, particularly above 30°, with a trend ($P = .1$) for native humeral heads to be closer to the joint midline (Figure 2, B). In light of these findings, we reject the hypothesis that concentric motion is achieved with all glenoids during scapular-plane elevation.

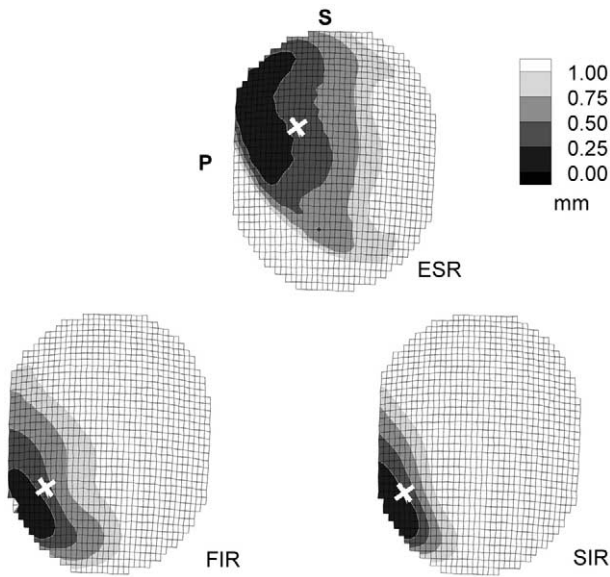


Figure 6 Representative contact map for conforming glenoid in eccentric loading positions. *White crosshairs* denote contact centroid. *S*, Superior; *P*, posterior.

Three additional loading positions (flexion, extension, and scapular-plane internal rotation) were selected to promote humeral head contact on or near the anterior-posterior glenoid rim. In response to these eccentric applied loads, the BF's ability to "contain" rim loading, given its hybrid design, was expected to be intermediate to that of the perfectly congruent and incongruent glenoids. As GHJs were progressively loaded from extension into flexion, despite the lack of statistically significant differences in humeral head kinematics, conforming joint contact centroids migrated closer to the posterior glenoid rim (Figure 5, A). Posterior translation has previously been shown in normal cadaveric joints in which simulated muscle forces were used to achieve flexion.⁷ We believe that the combined effects of muscle forces (Table I) and glenoid component geometry led to the observed patterns of posterior humeral translation in our study. The BF, natural joint, and nonconforming glenoids appeared to control rim loading under these eccentric loads when compared with the conforming glenoid ($P = .05$) (Figures 5, A, 6, 7, and 8). The similarity in contact patterns between the BF and nonconforming glenoids suggests that, under the experimental loading conditions, contact typically occurred in the outer, nonconforming portion of the BF (Figures 7 and 8). Interestingly, all glenoids exhibited contact primarily superior to the component center, although these centroids were no closer than 5 mm from the superior glenoid rim (Figure 5, B). We, therefore, confirm the hypothesis that eccentric loading of conforming implants produces contact near the glenoid edge. With

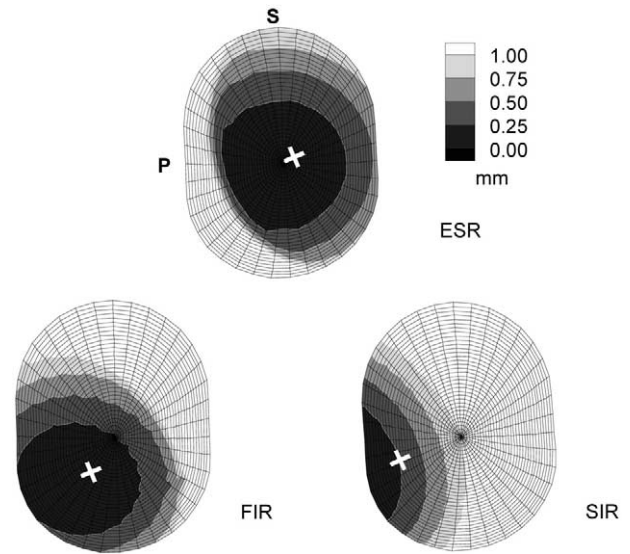


Figure 7 Representative contact map for nonconforming glenoid in eccentric loading positions. *White crosshairs* denote contact centroid. *S*, Superior; *P*, posterior.

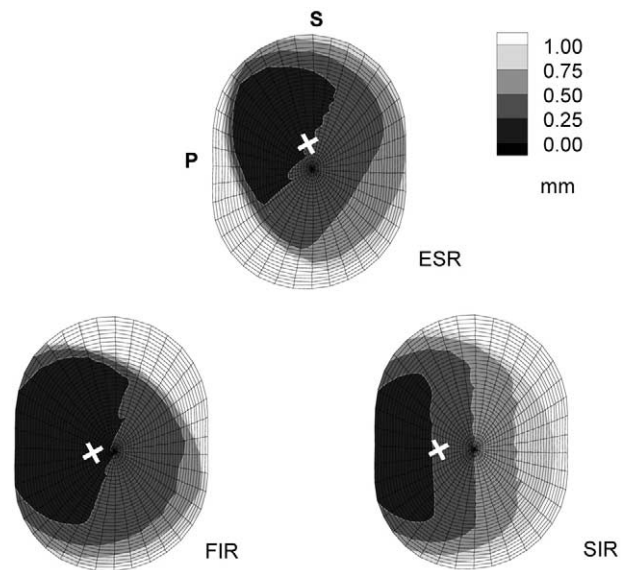


Figure 8 Representative contact map for variable conforming (ie, BF) glenoid in eccentric loading positions. *White crosshairs* denote contact centroid. *S*, Superior; *P*, posterior.

the numbers available, no significant differences in glenohumeral motion and contact could be detected among the BF and nonconforming designs as well as the natural joint.

Under conditions of uniformly applied muscle forces across the 4 test configurations, statistically significant differences in calculated resultant applied forces were found only with forward flexion, where the nonconforming design experienced greater pos-

terior loads than the natural joint ($P = .037$). The mean magnitude of the maximum resultant joint forces to which the implants were subjected in this study was 194 N (less than one-third body weight for a 76-kg individual). During independent experiments in our laboratory, a prosthetic humeral head was statically loaded (200 N) onto a mating glenoid by use of a servohydraulic testing system, and minimal (<0.15 mm) creep deformation of the polyethylene glenoids was noted. Therefore, it was not likely that ultrahigh-molecular weight polyethylene creep influenced the biomechanical results of the present study.

Care was taken to minimize confounding experimental variables during testing. We used a blinded and randomized testing approach for the prosthetic glenoids, and we could not attribute our results to testing sequence, as there did not exist meaningful disparities among glenoids. In each specimen, positioning of successive glenoid implants was consistent as a result of the minimal loss of bone associated with our recementing techniques. Hence, we do not believe that our results are attributable to glenoid malposition. The capsular release and repair, which were necessitated by our articular-surface registration techniques, were performed before any kinematic testing. A tight or lax capsule would be expected to alter joint motion with all glenoids, whereas in this study statistically significant posterior humeral migration was found only for the conforming glenoid. Additional pilot studies were conducted to investigate the influence of muscle forces on joint stability for the 7 test positions examined. We observed that incremental muscle force loading afforded a proprioceptive ability, in the sense that loads could be manually adjusted and balanced to prevent joint dislocation, particularly for eccentric loading positions. However, the capability to "sense" how well the humeral head was seated in the glenoid not only constituted a potential bias in experimentation but also resulted in substantial disparities in the magnitude of applied resultant force vectors across test configurations. Hence, we used a passive-assisted active muscle loading approach to maintain similar muscle force balancing throughout the course of testing of each shoulder specimen. At the same time, we recognize the possibility that a single combination of muscle forces may not have been conducive to stability for all implants. Indeed, this may have been the case for the conforming prosthetic joints, in which posterior kinematic and contact patterns were consistently noted across all experiments.

Few laboratory studies have examined the effect of component conformity on glenohumeral kinematics and contact patterns, although several investigations have reported subluxation or dislocation forces as measures of joint stability.^{1,23,33,45} Karduna et al³² used a human cadaveric model of TSA to quantify

translations in glenohumeral components whose radial mismatches varied from 0 through 5 mm. Under conditions of active loading, both S-I and A-P translations increased significantly with radial mismatch. The authors found that approximately 4 mm of mismatch on average best replicated normal joint translations. Meanwhile, a recent clinical study by Walch et al⁵⁰ reported that glenoid radiolucent lines (a potential indicator of component loosening) were less prevalent in joints with a radial mismatch greater than 5.5 mm but less than 10 mm. However, in this radiographic study, all implanted glenoids were flat-backed and thus more prone to edge loading. In our study, nonconforming glenoids (whose radii of curvature were 3 mm greater than those of the humeral head) exhibited no statistically significant differences, aside from the resultant joint force in flexion, compared with natural joints.

Our results suggest that glenohumeral stability is greater in natural joints compared with prosthetic joints. When the group mean of the 3 implants is considered, the center of curvature of the native humeral heads was significantly closer to the joint midline during scapular-plane elevation on the basis of S-I kinematics ($P = .017$) and A-P contact ($P = .0015$); under eccentric loading, similar trends were evident ($P = .0015$ and $P = .0038$, respectively). In contrast, when data only for radial mismatches up to 3 mm are examined, it is apparent that the A-P and S-I joint translations reported by Karduna et al³² were smaller for implants compared with natural joints. However, one must consider several key differences between our study and that of Karduna et al. The latter investigation focused on the positions of full internal to external humeral rotation at 90° arm elevation, used a surgical technique that preserved the integrity of the capsule, and found no significant differences in kinematics between natural joints and prosthetic joints whose radial mismatches ranged from 0 to 5 mm. The biomechanical differences between natural and prosthetic joints are likely attributable to the greater compliance of articular cartilage and labrum in comparison to polyethylene. For the native glenohumeral cartilage surfaces of the specimens evaluated in this investigation, the radial mismatch as determined from SPG analysis ranged from 0.7 to 2.4 mm, with a mean value of 1.4 ± 0.6 mm. In a natural glenohumeral articulation with a slight mismatch in humeral head and glenoid curvatures, deformation of cartilage during joint loading may actually increase the congruity of the joint and improve stability. This mechanism may explain the findings that joint contact centroids tended to be closer to the joint midline in natural relative to prosthetic joints.

In summary, despite clinical speculation that component conformity in TSA strongly influences implant performance and survival, in this investigation few

statistically significant ($P < .05$) differences were detected among 3 prosthetic glenoid designs under the imposed test conditions. The glenoid designs featuring some degree of mismatch behaved similarly to the natural joint, with no statistical differences in joint kinematics or contact patterns detected among these 3 test configurations. However, the conforming design led to posterior translation and contact near the glenoid rim. With regard to glenoid component complications, the 2 major mechanisms of clinical concern are elevated contact stresses producing polyethylene wear and edge loading leading to component loosening. Our finite-element studies previously demonstrated considerably increased contact stresses in fully nonconforming relative to fully conforming glenoids, as well as a benefit (ie, lowered stresses) to adding a partial region of conformity to a fully nonconforming glenoid. Our kinematic and contact data further suggest that adding a peripheral zone of translation to a fully conforming glenoid reduces the likelihood of rim loading, thereby increasing joint stability.

We wish to thank Matthew T. Sugalski, MD, Theodore A. Blaine, MD, Michael Q. Freehill, MD, William N. Levine, MD, Jeckin Shah, and Gopal Patel for their contributions to this study.

REFERENCES

1. Anglin C, Wyss UP, Pichora DR. Shoulder prosthesis subluxation: theory and experiment. *J Shoulder Elbow Surg* 2000;9:104-14.
2. Ateshian GA, Soslowsky LJ, Mow VC. Quantitation of articular surface topography and cartilage thickness in knee joints using stereophotogrammetry. *J Biomech* 1991;24:761-76.
3. Ateshian GA, Kwak SD, Soslowsky LJ, Mow VC. A stereophotogrammetric method for determining in situ contact areas in diarthrodial joints, and a comparison with other methods. *J Biomech* 1994;27:111-24.
4. Ateshian GA, Ark JW, Rosenwasser MP, et al. Contact areas in the thumb carpometacarpal joint. *J Orthop Res* 1995;13:450-8.
5. Barrett WP, Franklin JL, Jackins SE, Wyss CR, Matsen FA III. Total shoulder arthroplasty. *J Bone Joint Surg Am* 1987;69:865-72.
6. Bigliani LU, Weinstein DM, Glasgow MT, Pollock RG, Flatow EL. Glenohumeral arthroplasty for arthritis after instability surgery. *J Shoulder Elbow Surg* 1995;4:87-94.
7. Blasler RB, Soslowsky LJ, Malicky DM, Palmer ML. Posterior glenohumeral subluxation: active and passive stabilization in a biomechanical model. *J Bone Joint Surg Am* 1997;79:433-40.
8. Blevins FT, Pollo FE, Torzilli PA, Warren RF. Effect of humeral head component size on hemiarthroplasty translations and rotations. *J Shoulder Elbow Surg* 1998;7:591-8.
9. Brems JJ. The glenoid component in total shoulder arthroplasty. *J Shoulder Elbow Surg* 1993;2:47-54.
10. Buechel FF, Pappas MJ, DePalma AF. "Floating-socket" total shoulder replacement: anatomical, biomechanical, and surgical rationale. *J Biomed Mater Res* 1978;12:89-114.
11. Cofield RH. Total shoulder arthroplasty with the Neer prosthesis. *J Bone Joint Surg Am* 1984;66:899-906.
12. Cofield RH, Edgerton BC. Total shoulder arthroplasty: complications and revision surgery. *Instr Course Lect* 1990;39:449-62.
13. Cofield RH. Revision procedures for shoulder arthroplasty. In: Morrey BF, editor. *Reconstructive surgery of the joints*. 2nd ed. New York: Churchill Livingstone; 1996. p. 789-99.
14. Collins DN, Harryman DT II. Arthroplasty for arthritis and rotator cuff deficiency. *Orthop Clin North Am* 1997;28:225-39.
15. Cotton RE, Rideout DF. Tears of the humeral rotator cuff: a radiological and pathological necropsy survey. *J Bone Joint Surg Br* 1964;46:314-28.
16. Doody SG, Freedman L, Waterland JC. Shoulder movements during abduction in the scapular plane. *Arch Phys Med Rehabil* 1970;51:595-604.
17. Flatow EL, Ateshian GA, Soslowsky LJ, et al. Computer simulation of glenohumeral and patellofemoral subluxation. *Clin Orthop* 1994;306:28-33.
18. Flatow EL. Prosthetic design considerations in total shoulder arthroplasty. *Semin Arthroplasty* 1995;6:233-44.
19. Flatow EL, Raimondo RA, Kelkar R, et al. Active and passive restraints against superior humeral translation: the contributions of the rotator cuff, the biceps tendon, and the coracoacromial arch [abstract]. *J Shoulder Elbow Surg* 1996;5:S111.
20. Franklin JL, Barrett WP, Jackins SE, Matsen FA III. Glenoid loosening in total shoulder arthroplasty. Association with rotator cuff deficiency. *J Arthroplasty* 1988;3:39-46.
21. Freedman L, Munro RR. Abduction of the arm in the scapular plane: scapular and glenohumeral movements. *J Bone Joint Surg Am* 1966;18:1503-10.
22. Friedman RJ. Glenohumeral translation after total shoulder arthroplasty. *J Shoulder Elbow Surg* 1992;1:312-6.
23. Fukuda K, Chen CM, Cofield RH, Chao EY. Biomechanical analysis of stability and fixation strength of total shoulder prostheses. *Orthopedics* 1988;11:141-9.
24. Gardner TR, Ateshian GA, Grelsamer RP, Mow VC. A 6 DOF knee testing device to determine patellar tracking and patellofemoral joint contact area via SPG. *ASME Adv Bioeng* 1994;BED28:279-80.
25. Green A, Norris TR. Shoulder arthroplasty for advanced glenohumeral arthritis after anterior instability repair. *J Shoulder Elbow Surg* 2001;10:539-45.
26. Cristina AG, Romano RL, Kammire GC, Webb LX. Total shoulder replacement. *Orthop Clin North Am* 1987;18:445-53.
27. Harryman DT, Sidles JA, Harris SL, Lippitt SB, Matsen FA III. The effect of articular conformity and the size of the humeral head component on laxity and motion after glenohumeral arthroplasty. A study in cadavera. *J Bone Joint Surg Am* 1995;77:555-63.
28. Harryman DT II, Sidles JA, Clark JM, et al. Translation of the humeral head on the glenoid with passive glenohumeral motion. *J Bone Joint Surg Am* 1990;72:1334-43.
29. Howell SM, Galinat BJ, Renzi AJ, Marone PJ. Normal and abnormal mechanics of the glenohumeral joint in the horizontal plane. *J Bone Joint Surg Am* 1988;70:227-32.
30. Iannotti JP, Williams GR. Total shoulder arthroplasty. Factors influencing prosthetic design. *Orthop Clin North Am* 1998;29:377-91.
31. Karduna AR, Williams GR, Williams JL, Iannotti JP. Kinematics of the glenohumeral joint: influences of muscle forces, ligamentous constraints, and articular geometry. *J Orthop Res* 1996;14:986-93.
32. Karduna AR, Williams GR, Williams JL, Iannotti JP. Glenohumeral joint translations before and after total shoulder arthroplasty. A study in cadavera. *J Bone Joint Surg Am* 1997;79:1166-74.
33. Karduna AR, Williams GR, Williams JL, Iannotti JP. Joint stability after total shoulder arthroplasty in a cadaver model. *J Shoulder Elbow Surg* 1997;6:506-11.
34. Karduna AR, Williams GR, Iannotti JP, Williams JL. Total shoulder arthroplasty biomechanics: a study of the forces and strains at the glenoid component. *J Biomech Eng* 1998;120:92-9.
35. Kelkar R. Normal and abnormal mechanics of the shoulder: studies of articular geometry, contact and kinematics [PhD thesis]. New York: Columbia University; 1996.
36. Kelkar R, Wang VM, Flatow EL, et al. Glenohumeral mechanics: a study of articular geometry, contact, and kinematics. *J Shoulder Elbow Surg* 2001;10:73-84.

37. Kronberg M, Nemeth G, Brostrom LA. Muscle activity and coordination in the normal shoulder. An electromyographic study. *Clin Orthop* 1990;257:76-85.
38. Neer CS II, Watson KC, Stanton FJ. Recent experience in total shoulder replacement. *J Bone Joint Surg Am* 1982;64:319-37.
39. Neer CS II. Glenohumeral arthroplasty. In: Reines L, editor. *Shoulder reconstruction*. Philadelphia: Saunders; 1990. p. 143-362.
40. Noble JS, Bell RH. Failure of total shoulder arthroplasty: why does it occur? *Semin Arthroplasty* 1995;6:280-8.
41. Otis JC, Jiang CC, Wickiewicz TL, et al. Changes in the moment arms of the rotator cuff and deltoid muscles with abduction and rotation. *J Bone Joint Surg Am* 1994;76:667-76.
42. Pollock RG, Deliz ED, McIlveen SJ, Flatow EL, Bigliani LU. Prosthetic replacement in rotator cuff deficient shoulders. *J Shoulder Elbow Surg* 1992;1:173-86.
43. Poppen NK, Walker PS. Normal and abnormal motion of the shoulder. *J Bone Joint Surg Am* 1976;58:195-201.
44. Rodosky MW, Bigliani LU. Indications for glenoid resurfacing in shoulder arthroplasty. *J Shoulder Elbow Surg* 1996;5:231-48.
45. Severit R, Thomas BJ, Tsenter MJ, Amstutz HC, Kabo JM. The influence of conformity and constraint on translational forces and frictional torque in total shoulder arthroplasty. *Clin Orthop* 1993;292:151-8.
46. Soslowsky IJ, Flatow EL, Bigliani LU, Mow VC. Articular geometry of the glenohumeral joint. *Clin Orthop* 1992;285:181-90.
47. Soslowsky IJ, Flatow EL, Bigliani LU, et al. Quantitation of in situ contact areas at the glenohumeral joint: a biomechanical study. *J Orthop Res* 1992;10:524-34.
48. Torchia ME, Cofield RH, Settergren CR. Total shoulder arthroplasty with the Neer prosthesis: long-term results. *J Shoulder Elbow Surg* 1997;6:495-505.
49. Vaesel MT, Olsen BS, Sojbjerg JO, Helming P, Sneppen O. Humeral head size in shoulder arthroplasty: a kinematic study. *J Shoulder Elbow Surg* 1997;6:549-55.
50. Walch G, Edwards TB, Boulahia A, et al. The influence of glenohumeral prosthetic mismatch on glenoid radiolucent lines: results of a multicenter study. *J Bone Joint Surg Am* 2002;84:2186-91.
51. Wang VM, Sugalski MT, Pawluk RJ, Levine WN, Mow VC. Effects of humeral rotation on normal glenohumeral kinematics and joint reaction forces. *Trans Orthop Res Soc* 2000;25:407.
52. Williams M, Lissner HR. *Biomechanics of human motion*. 2nd ed. Philadelphia: Saunders; 1977. pp. 206-210.
53. Wirth MA, Rockwood CA Jr. Complications of total shoulder-replacement arthroplasty. *J Bone Joint Surg Am* 1996;78:603-16.
54. Zimmer, Inc. Bigliani/Flatow, the complete shoulder solution: total shoulder arthroplasty surgical technique. Warsaw (IN): Zimmer, Inc; 2001.